Volume 4 | Number 9 | September 2014 | Pages 2687–3394

Catalysis Science & Technology

www.rsc.org/catalysis

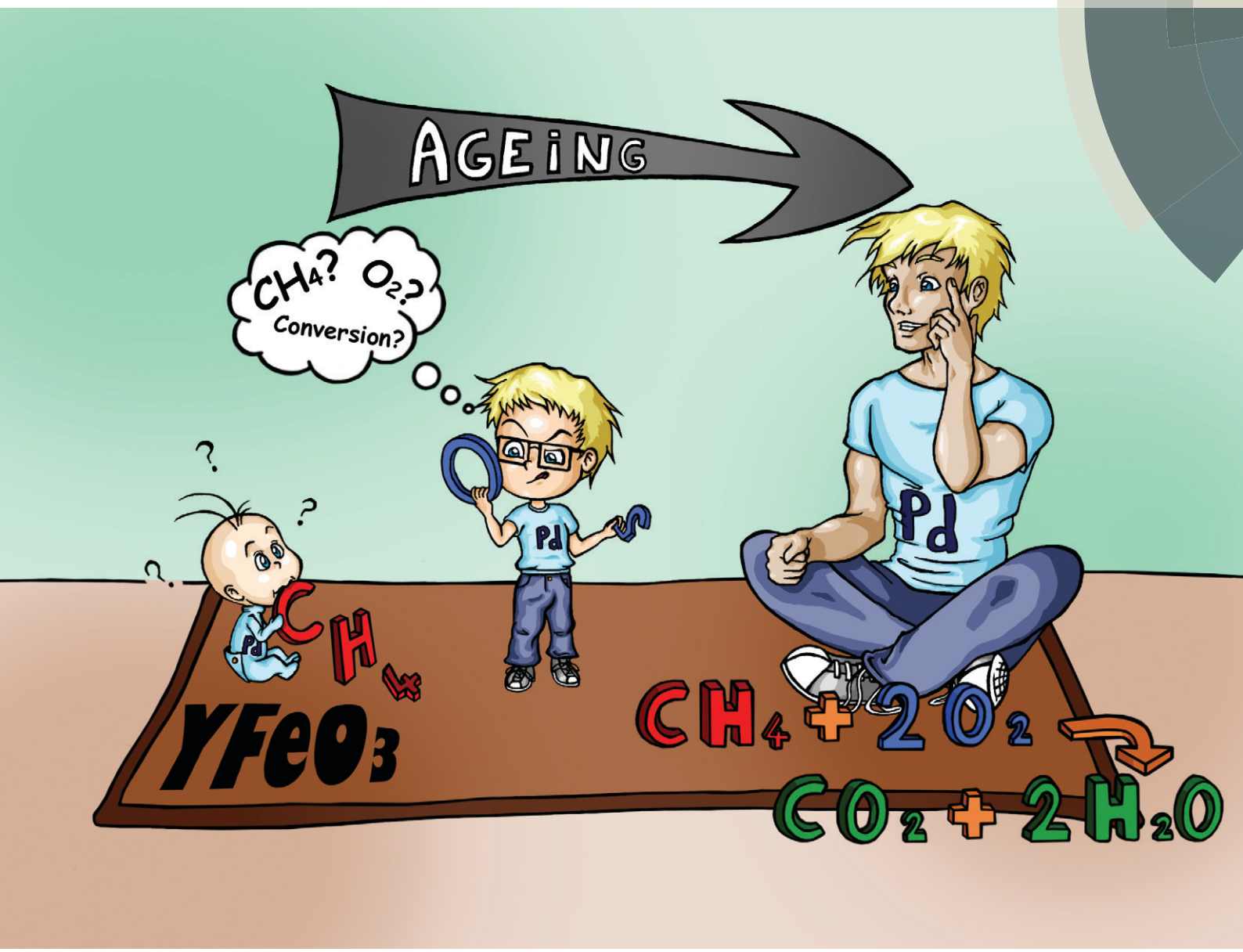

ISSN 2044-4753

ROYAL SOCIETY OF CHEMISTRY

PAPER
Ferri *et al.*
Ageing induced improvement of methane oxidation activity of $Pd/YFeO_3$

Catalysis Science & Technology

PAPER

View Article Online
View Journal | View Issue

Cite this: *Catal. Sci. Technol.*, 2014, **4**, 2919

Ageing induced improvement of methane oxidation activity of $Pd/YFeO_3$

Ye Lu,[a] Sylvain Keav,[a] Valentina Marchionni,[b] Gian Luca Chiarello,†[a] Alfonsina Pappacena,[c] Marco Di Michiel,[d] Mark A. Newton,[d] Anke Weidenkaff‡[a] and Davide Ferri*[b]

The ageing characteristics of flame-made 2 wt% Pd supported on $YFeO_3$ were analysed in comparison with a Pd/Al_2O_3–CeO_2–ZrO_2 three-way catalyst (TWC) with respect to structural changes and catalytic performance for methane oxidation under stoichiometric reaction conditions. Thermal treatment under lean conditions (air, 900 °C) resulted in slight decrease in the methane oxidation activity of the TWC. In marked contrast, $YFeO_3$-supported Pd catalysts exhibit an increase in activity after such treatment. Activity enhancement is even higher when the treatment was performed under stoichiometric conditions (air–fuel equivalence ratio, $\lambda = 1$, 900 °C). To explain this observation, in-depth characterization (BET, STEM, OSCC, XAS, and CO chemisorption) of fresh and aged catalysts was performed. Both thermal and stoichiometric ageing cause a severe sintering of the support particles and the phase transformation from hexagonal to orthorhombic $YFeO_3$. Despite the absence of a mixed Pd–$YFeO_3$ phase, the growth of Pd particles appears to be limited under the $\lambda = 1$ atmosphere. In contrast to thermally aged catalysts where large PdO particles are formed, well-defined metallic Pd nanoparticles of 10–20 nm are present after stoichiometric ageing along with higher methane oxidation activity. Although it is tempting to conclude that metallic Pd is active for methane oxidation under the given conditions, reversible and periodic partial oxidation of the large metallic particles is observed in modulation excitation high energy X-ray diffraction (HXRD) experiments designed to simulate the oscillating redox conditions experienced during operation. These results indicate that large Pd particles exhibit improved methane oxidation activity but equally confirm that activity under stoichiometric conditions is the result of a delicate equilibrium dictated by the bulk-Pd/surface-PdO pair.

Received 7th March 2014,
Accepted 10th April 2014

DOI: 10.1039/c4cy00289j

www.rsc.org/catalysis

Introduction

The exhaust of modern stoichiometric engines fuelled with natural gas is controlled using Pd-based three-way catalysts (TWC).[1] Pd is considered the precious metal of choice for oxidation of methane,[2,3] the major component of natural gas. During operation, the atmosphere around the TWC is periodically varied between slightly reducing and slightly oxidizing that allows maintenance of the emission levels within those demanded by the existing stringent regulations.[4] Although the TWC for natural gas vehicles is typically derived from the gasoline TWC, their chemistries can display significant differences.[5,6] However, similarly to its gasoline counterpart, the TWC for natural gas applications suffers from deleterious ageing effects. Its activity progressively declines with mileage as a result of several intersecting phenomena such as thermal deactivation upon exposure to temperatures as high as 1000 °C and poisoning by fuel additives and impurities.[7–14] Therefore, the growing interest in natural gas, bio-gas and synthetic natural gas as interim CO_2-poor fuel has driven efforts aiming at designing tailored TWC systems for this specific application.

PdO is considered essential for CH_4 oxidation under lean conditions.[15] Selection of an appropriate oxidic support stabilizes Pd^{2+} against spontaneous reduction at high temperature.[16–18] The decomposition of PdO to Pd is considered to cause catalyst deactivation during reaction.[19–21] The role of metallic Pd remains an interesting and much debated issue,[22] which is even more fundamental in the case of the TWC because of the oscillating redox reaction conditions. Metallic Pd is observed by X-ray absorption spectroscopy on a model TWC comprising

[a] *Empa, Swiss Federal Laboratories for Materials Science and Technology, Laboratory for Solid State Chemistry and Catalysis, Ueberlandstrasse 129, CH-8600 Dübendorf, Switzerland*
[b] *Paul Scherrer Institut, CH-5232 Villigen PSI, Switzerland. E-mail: davide.ferri@psi.ch; Tel: +41 56 310 2781*
[c] *Università di Udine, Dipartimento di Scienze e Tecnologie Chimiche, via Cotonificio 108, I-33100 Udine, Italy*
[d] *ESRF, 71 Rue des Martyrs, F-38000 Grenoble*
† Present address: Università degli Studi di Milano, Dipartimento di Chimica, via C. Golgi 19, I-20133 Milano, Italy.
‡ Present address: Institute for Materials Science, University of Stuttgart, Heisenbergstrasse 3, DE-70569 Stuttgart, Germany.

Al_2O_3 and ceria–zirconia when the catalyst is exposed to high temperature (800–900 °C)[5] and a mixed PdO–Pd state needs to be accounted for in light-off experiments under stoichiometric reaction conditions with methane as the hydrocarbon.[23] Pd reduction and sintering can be partly prevented by the formation of PdO at increasing O_2 concentration, for example during fuel cut-off.[24] However, methane oxidation activity under lean conditions was recently shown to increase linearly with Pd particle size ranging from 1 to 20 nm,[25] which is in line with previous observations.[26,27] Ageing under reaction conditions ($O_2 : CH_4 = 4$) also produced a more active Pd/Al_2O_3 with larger Pd particles (7–16 nm).[28] Restructuring of PdO crystallites upon reduction resulted in increased catalytic activity.[15,29,30]

Perovskite-type oxides of the general formula ABO_3 have long been recognized as oxidation catalysts[31–34] and reported as potential NO_x storage/reduction catalysts (NSR),[35] TWC,[36–38] soot combustion catalysts[39] and catalysts for natural gas lean burn engines.[40] In addition, they are also promising oxygen storage materials.[37,41,42] In line with the search for metal oxides able to stabilize Pd^{2+} against reduction, they can host noble metals in an unusual oxidation state within their lattice. As a direct consequence, in terms of potential TWC components they offer the possibility of stabilizing Pd against sintering under the redox oscillations experienced during operation as has been demonstrated for use with gasoline engines.[43] In a very similar way, formation of a Pt-containing perovskite-type oxide ($BaPtO_3$ and Ba_2CePtO_6) after ageing of the $Pt/Ba/CeO_2$ NSR catalyst was shown to maintain Pt in a well dispersed state, with the reduced Pt state and the activity being able to be restored after mild reduction.[44] Despite the growing literature on the topic, which often assumes that the noble metal will adopt the coordination state of the B-site cation, and criticism of the self-regenerative function,[45] this property needs to be considered with care as it most likely exists within only a limited choice of phase compositions[46–49] and is clearly temperature dependent.[43] Nevertheless, even in the absence of noble metal incorporation, $LaFeO_3$ is able to exert a strong stabilization effect that makes Pt more resistant against thermal ageing and consequently more active than when it is deposited on γ-Al_2O_3.[50] Recently, hexagonal $YFeO_3$ has been shown to be a promising host for Pd for CO oxidation[51] and for methane oxidation under lean[52] and stoichiometric conditions.[53] $YFeO_3$ was shown to be superior to $YMn_{0.5}Fe_{0.5}O_3$ with respect to the reversible incorporation of Pd within the $YFeO_3$ lattice.[48] $YFe_{1-x}Pd_xO_{3-\delta}$ (x = 0.1) exhibited the self-regenerative property at temperatures below 500 °C where the coordinatively unsaturated Pd reversibly segregates out of and re-incorporates within $YFeO_3$ in consecutive redox treatments.[51] Further, the coordination of Pd with $YFeO_3$ changes at high temperature. The fine dispersion of Pd in the catalyst after calcination at 700 °C, where Pd is likely in the coordination state that leads to the self-regenerative CO oxidation catalyst,[51] is lost after calcination at 800 °C in favour of segregated PdO, while the hexagonal structure (of the support) is still maintained.[52] Well dispersed Pd nanoparticles on $YFeO_3$ grow to well defined particles of *ca.* 20 nm after repeated methane oxidation cycles under stoichiometric conditions,[54] questioning the protective function of the perovskite-related material in case of high temperature treatments of $YFeO_3$. However, activity enhancement for methane oxidation was observed in parallel to the formation of the 20 nm Pd particles. Such an enhancement has been reported also for the La–Mn–Ce–Pd–O perovskite-type oxide where Pd is observed to segregate after ageing under simulated exhaust of a natural gas engine.[55]

Given the increased methane oxidation activity of $Pd/YFeO_3$ after exposure to 850 °C concurrent to the growth of Pd particles that suggests possible activation after ageing, herein we address the structure and the catalytic performance of flame-made 2 wt% $Pd/YFeO_3$ after treatment under lean and stoichiometric conditions at 900 °C. A sample of $Pd/YFeO_3$ with four-fold lower Pd content was also prepared and aged under identical conditions. The methane oxidation activity under stoichiometric conditions is compared with that of a conventional model TWC.

Experimental

Catalyst synthesis

$Pd/YFeO_3$ (nominal 0.5 and 2 wt% Pd) was synthesized by flame spray synthesis (FSS) using an acetylene flame. Briefly, a mixture of deionized water and *N*,*N*-dimethylformamide (DMF, 99%, Sigma-Aldrich, 1 : 3) was used as solvent of the metal nitrate precursors and sprayed in an acetylene–air flame.[53] After synthesis, the samples were calcined in air at 700 °C for 2 h. The powder TWC was composed of Pd, alumina and ceria–zirconia (Pd/ACZ; 1.6 wt% Pd; calcined at 500 °C; SSA = 135 $m^2\ g^{-1}$) and was kindly provided by Umicore.

Heat treatments, in the following designated concisely as ageing, were carried out at 900 °C for 2 h. Thermal ageing (A_T) was carried out in static air, while stoichiometric ageing (A_S) was performed using a gas mixture comprising 7000 ppm CO, 1300 ppm CH_4, 1600 ppm NO_x and 5300 ppm O_2 in He (λ = 1) at 100 mL min^{-1} in the plug-flow reactor used for catalytic activity measurements. In the following, the samples are labelled 2Pd/YFO-x, 0.5Pd/YFO-x and Pd/ACZ-x, where x is F (fresh), A_T or A_S.

Characterization

The specific surface area was determined by the single-point BET method in 30 vol% N_2/He using a QuantaChrome ChemBET 3000 instrument. Prior to measurements, all samples were degassed in pure N_2 at 200 °C for 30 min.

The phase composition of fresh and aged catalysts was analysed by X-ray diffraction (X'Pert Pro PANalytical) using monochromatic Cu Kα_1 radiation (λ = 1.54 Å). The diffraction patterns were recorded between 20° and 80° (2θ) with an angular step interval of 0.0167°. Phase identification was performed using the ICDD reference database in the X'Pert HighScore Plus software.

The morphology of the catalysts was observed using a Jeol 2200FS transmission electron microscope equipped with a 200 kV field emission gun and a high-angle annular dark

field detector in STEM mode providing images with atomic number ($Z^{1.5-1.8}$) contrast.[56] The local composition was determined by energy dispersive X-ray spectroscopy (EDS). The samples were prepared by evaporation of an alcohol suspension on a copper grid coated with a holey carbon film. The palladium particle size distribution was obtained by measuring up to 200 particles using the software ImageJ.[57]

The oxygen storage capacity complete (OSCC) defined as the total amount of desorbed oxygen was determined under static conditions using the thermogravimetric method.[58,59] The samples were treated with 5 vol% H_2/Ar at 400 °C for 70 min using a TGA Q500 setup (TA Instruments). The measured weight loss was converted into the corresponding oxygen content assuming that the sample is fully oxidized in its initial state.

Diffuse reflectance infrared Fourier transform spectroscopy (DRIFTS) data were collected at a resolution of 4 cm^{-1} using a VERTEX 70 FT-IR spectrometer (Bruker) equipped with a high temperature reaction chamber (HVC-DRP2, Harrick) and a liquid-nitrogen cooled MCT detector. Prior to CO adsorption, the samples were exposed to 20 vol% O_2/Ar (50 mL min^{-1}) at 500 °C for 30 min, followed by reduction at 300 °C for 30 min in 10 vol% H_2/Ar. After changing to Ar and cooling to room temperature, a background spectrum was obtained prior to CO adsorption in 5 vol% CO/Ar.

Extended X-ray absorption fine structure (EXAFS) spectroscopy data were obtained in the transmission mode at the Pd K-edge (24.35 keV) at the SuperXAS beamline of the Swiss Light Source (PSI, Switzerland). The spectrum of the Pd foil was simultaneously collected for energy calibration. The required sample amount was homogeneously mixed with polyethylene and pressed into pellets. The spectra were energy and background corrected and normalized with the software Athena.[60]

Time-resolved high energy XRD data (86.8 keV, λ = 0.143 Å, $\Delta E/E \sim 1.4 \times 10^{-3}$) were collected at beamline ID15B of the ESRF (Grenoble, France) using a digital flat 2D panel detector (Pixium 4700) mounted at 900 mm from the sample position. In a concentration modulation experiment, the sample was mounted in a homemade stainless steel cell and was subjected to a sequence of 50 alternate and equally long pulses (25 s) of 1 vol% O_2/He and 1 vol% CO/He at 400 °C at 100 mL min^{-1}.[61] A series of 100 time-resolved diffraction patterns were collected during a full modulation period (T = 50 s). The catalyst powder (*ca.* 50 mg, 50–100 μm) was fixed between two quartz wool plugs in a homemade stainless steel reactor cell equipped with graphite windows. The temperature of the sample was recorded using a thermocouple inserted at the entrance of the catalyst bed and was constant within ±1 °C during the isothermal pulse experiment. The outlet of the cell was connected to a mass spectrometer (OmniStar, Pfeiffer) that was used to follow signals of m/z 28 (CO), 32 (O_2), 44 (CO_2) and 4 (He) and simultaneously to read the sample temperature. The 5000 time-resolved XRD data collected in each experiment were averaged over the number of modulation periods into a single period prior to phase sensitive detection (PSD):

$$I_k^{\varphi^{\mathrm{PSD}}} = \frac{2}{T}\int_0^T I(t)\sin(k\omega t + \varphi_k^{\mathrm{PSD}})\mathrm{d}t \quad (1)$$

where T is the length of the modulation period, ω is the stimulation frequency, k is the demodulation index, φ_k^{PSD} is the phase angle, and $I(t)$ is the intensity of a reflection recorded as a function of reciprocal lattice vector ($Q = 4\pi\sin(\theta/2)/\lambda$, with θ being the scattering angle and λ the wavelength of the incident radiation) and time.[62–64] According to the theory of modulation enhanced diffraction,[65] the integral of eqn (1) can be more explicitly (and correctly) written to contain two terms, one of which depends only on the component of the system that is stimulated, whereas the second one contains both this component and the static one. PSD with k = 2 should provide only the response of the former component, but we did not find any difference other than intensity by using k = 1, which is shown here. The Simpson series was used to calculate the integral of eqn (1). The resulting new set of phase-resolved data contains only the response of species responding with the same frequency of the external stimulation. A critical point is that the changes must be reversible to the external stimulus, for example a change in concentration of the gas phase. PSD removes static signals – typically overwhelming – thus revealing the information pertaining to what are often weak signals. This method is especially useful to study real catalysts with relevant (low) Pd content, which is either silent or unlikely to be distinguished using conventional spectroscopic/diffraction methods. The resulting new set of phase-resolved data essentially contains the response of the signals (species) that are responding with the same frequency of the external stimulation (CO *vs.* O_2 concentration modulation) and on the delay with which they respond to the external stimulus.

Three-way catalytic activity

The light-off of the catalysts was measured in an exhaust mixture comprising 7000 ppm CO, 1300 ppm CH_4, 1600 ppm NO_x and 5300 ppm O_2 (He balance; 100 mL min^{-1}) between 25 °C and 850 °C. The measurements were carried out in a quartz-tube reactor (d = 6 mm) using catalyst particles (150–200 μm; 100 mg) diluted with the same volume of sea sand and firmly fixed in the middle of the reactor between two quartz wool plugs. Prior to the reaction, the catalysts were treated in 20 vol% O_2/He (50 mL min^{-1}) at 700 °C for 2 h. The gas hourly space velocity (GHSV) was approximately 60 000 h^{-1}. The outlet of the reactor was analysed using a gas chromatograph (Agilent 3000A Micro GC) equipped with two columns (PoraPLOT-Q for CH_4, CO_2, H_2O and N_2O; molecular sieve 5 Å for CO and NO).

Results and discussion

Characterization of fresh and aged catalysts

The structural properties of fresh and aged catalysts are summarized in Table 1. The phase composition of each sample was determined by XRD. Since the same crystal phases were identified in 0.5Pd/YFO and 2Pd/YFO, only the XRD patterns of 2Pd/YFO and Pd/ACZ are presented in Fig. 1. 2Pd/YFO-F

exhibits the patterns of hexagonal $YFeO_3$, while no information is obtained on the Pd-containing phase due to the overlap with the $YFeO_3$ phase and its good dispersion (Table 1).[53] Irrespective of the ageing atmosphere, hexagonal $YFeO_3$ is converted into the orthorhombic phase, which was reported to occur around 800 °C.[66–68] Despite the high temperature treatment, no evidence of the presence of a Pd-containing phase is obtained. On the contrary, the inset of Fig. 1 demonstrates that metallic Pd is formed as a consequence of stoichiometric ageing. The Pd(111) and Pd(200) reflections of fcc-Pd appear at *ca.* 40 and 47°, respectively. The phase transition of $YFeO_3$ upon exposure to 900 °C is accompanied by a considerable loss of surface area (Table 1). Likely as a consequence of both phase transition and particle growth processes, the oxygen storage capacity complete (OSCC) is also severely diminished compared to the remarkable value measured for the fresh catalyst. The OSCC values of the aged 2Pd/YFO catalysts are *ca.* ten times higher than that of the thermally aged support suggesting that the OSCC of the aged catalysts is primarily dictated by the presence of Pd. This is also confirmed by the decreased OSCC value obtained with lower Pd loading that is still *ca.* 4–8 times higher than that of the support depending on the ageing procedure.

For comparison, the XRD patterns of fresh and aged Pd/ACZ (Fig. 1) correspond to those of γ-Al_2O_3 and cubic CZ and are very similar, confirming the thermal stability of ACZ.[69] However, the general sharpening of the diffraction peaks of CZ after both ageing procedures is indicative of some extent of sintering. This is especially evident in Pd/ACZ-A_T and is confirmed by the larger extent of surface area loss of this sample compared to Pd/ACZ-A_S. A (weak) peak corresponding to PdO becomes visible at *ca.* 55° in Pd/ACZ-A_T as well. Similarly to 2Pd/YFO-A_S, the XRD pattern of Pd/ACZ-A_S shows reflections of metallic Pd (peaks at 40 and 47°), confirming the reduction of Pd under these conditions.

HAADF-STEM was used to confirm the textural changes occurring upon ageing and to characterize the morphology of the Pd-containing phase. The STEM images of 2Pd/YFO are shown in Fig. 2d–f. Identical conclusions can be drawn for 0.5Pd/YFO (Fig. 2g–i). The sintering of $YFeO_3$ after exposure

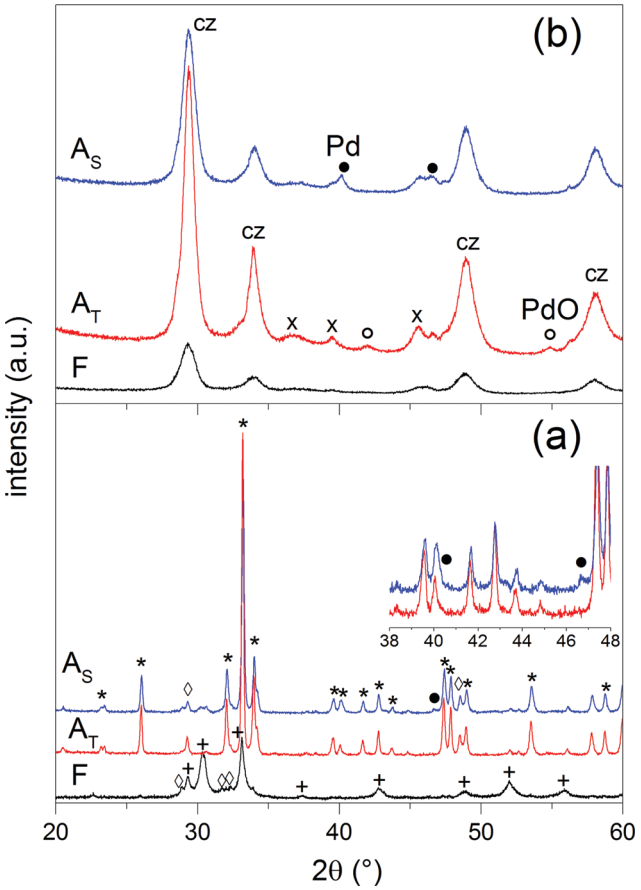

Fig. 1 XRD patterns of fresh and aged (a) 2Pd/YFO and (b) Pd/ACZ. (*) Orthorhombic $YFeO_3$, (+) hexagonal $YFeO_3$, (◊) Y_2O_3, (×) γ-Al_2O_3, (cz) ceria–zirconia, (●) Pd, and (○) PdO.

to 900 °C is rather obvious from these data. Similarly, Pd particle growth is also observed to be accompanied by a change in shape that depends on the ageing procedure. Pd particles appear mostly 'wetting' and spreading on $YFeO_3$ after thermal ageing (Fig. 2e; Table 1). Plate-like Pd particles were observed to form in an oxygen containing environment at $T > 800$ °C on Al_2O_3, while re-dispersion of Pd occurred on more coordinating metal oxides such as ZrO_2.[70] However,

Table 1 Structural properties of fresh and aged catalysts

Entry	Condition	SSA (m^2 g^{-1})	XRD[a]	OSCC[b] (μmol O_2 g^{-1})	Particle size[c] (nm)
Pd/ACZ	F	135	ACZ	150	8 [3]
	A_T	70	ACZ + PdO	157	52 [27]
	A_S	97	ACZ + Pd	188	13 [4.4]
2Pd/YFO	F	19	h + Y_2O_3[d]	504	3.5 [1.4]
	A_T	3	o + Y_2O_3 + h	86	91 [35]
	A_S	6	o + Y_2O_3 + h	88	19 [7.6]
0.5Pd/YFO	F	18	h + Y_2O_3[d]	424	—
	A_T	3	o + Y_2O_3 + h	39	101 [37.5]
	A_S	6	o + Y_2O_3 + h	67	18 [5.7]
YFO	F[e]	19	h + Y_2O_3[d]	416	—
	A_T	3	o + Y_2O_3 + h	8	—

[a] h: hexagonal, o: orthorhombic. [b] Oxygen storage capacity complete, determined by TG analysis. [c] Average Pd particle size estimated by STEM. The standard deviation σ is shown in brackets. [d] Metastable monoclinic Y_2O_3. [e] See ref. 53.

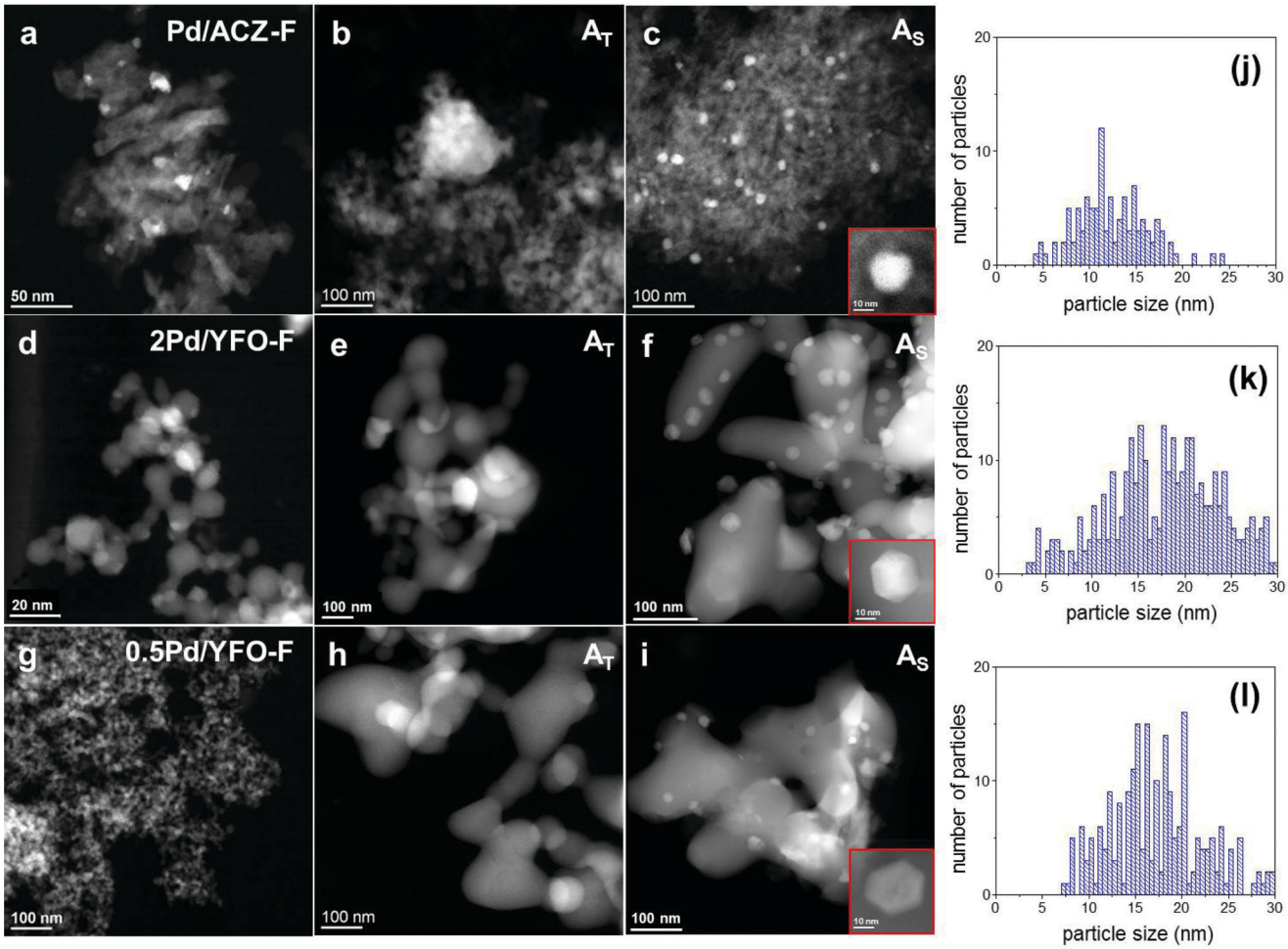

Fig. 2 HAADF-STEM images of fresh and aged (a–c) Pd/ACZ, (d–f) 2Pd/YFO, and (g–i) 0.5Pd/YFO and particle size distributions of (j) Pd/ACZ-A_S, (k) 2Pd/YFO-A_S and (l) 0.5Pd/YFO-A_S. F, fresh; A_T, thermal ageing; A_S, stoichiometric ageing.

the particles are not always easily recognizable and preclude any correct determination of particle size distribution. Assuming that the shape of Pd particles present in 2Pd/YFO-A_T is similar to that on Al_2O_3, this would indicate that the anchoring nature of $YFeO_3$ is lost upon ageing, in agreement with recent observations on Pd/$YFeO_3$ calcined at 700 °C and 800 °C.[52] The average particle size of the finely dispersed fresh catalyst increases from *ca.* 3.5 nm to *ca.* 19 nm in 2Pd/YFO-A_S (Fig. 2f) and the particle size distribution broadens (Table 1). Additionally, Pd nanoparticles with a different morphology from those obtained upon thermal ageing are obtained. The large fraction of hexagonal projections detected in the STEM images indicates that Pd particles possess a (truncated) cubo-octahedral shape exposing (111) and (100) facets.[71] The change in morphology upon stoichiometric ageing is similar to the one observed after three reaction cycles under $\lambda = 1$ conditions.[53] Hence, structural changes after repeated reaction cycles and stoichiometric ageing are of similar nature.

The different particle shape and the smaller particle size observed for 2Pd/YFO-A_S confirm previous results obtained on Pt/Al_2O_3 catalysts used for NO oxidation that were thermally aged at 800 °C or under a simulated lean diesel environment (propene, CO, NO_x and O_2) at the same temperature for 5 h.[72] Ageing under reaction conditions caused formation of truncated cubo-octahedral Pt particles with reduced size compared to the thermally aged catalyst. Hence, ageing under a reactive atmosphere produces smaller particles than thermal ageing at the same temperature.[73]

The STEM observations on the evolution of the structure of the Pd phase on $YFeO_3$ are confirmed and compared with the analysis of the Pd/ACZ reference catalyst. No significant change in the size of the metal oxide is observed that could support the variations of XRD intensity. The average Pd particle size increases from 8 nm in Pd/ACZ-F to 52 nm in Pd/ACZ-A_T (Fig. 2a and b). The growth of Pd particles is again less severe under stoichiometric conditions, with the average particle diameter being 13 nm in Pd/ACZ-A_S. Both round-shaped and truncated particles can be found in this sample (Fig. 2c). The particle size distribution of Pd/ACZ by STEM is, however, greatly influenced by Pd particles deposited on CZ that are difficult to detect.

The oxidation state and coordination environment of Pd were investigated by X-ray absorption spectroscopy. The XANES spectra of fresh and aged 2Pd/YFO and Pd/ACZ recorded at

the Pd K-edge are shown in Fig. 3a. The spectra of a Pd foil and bulk PdO are also given for reference. No detectable metallic Pd is present in the fresh catalyst.[53] The white line of 2Pd/YFO-F is very close to that of Pd/ACZ-F which is typical of a supported PdO catalyst. Nevertheless, the non-phase shift corrected k^3-weighted Fourier transform EXAFS spectrum of 2Pd/YFO-F (Fig. 3b) presents only a clear Pd–O coordination shell at 1.6 Å, while the second Pd–O–Pd shell clearly appears in Pd/ACZ-F at *ca.* 3.0 Å. The difference is due to the smaller particle size measured for the YFO-based catalyst (Table 1). The XANES and FT-EXAFS data of the thermally aged catalysts are also characteristic of PdO, but the stronger contribution of the Pd–O–Pd shell compared to the fresh catalysts confirms PdO particle growth upon ageing. After stoichiometric ageing, the presence of the Pd–Pd coordination shell at 2.5 Å at the expense of the Pd–O phase characterizes the 2Pd/YFO and Pd/ACZ catalysts. This confirms that Pd is in the metallic state, in agreement with the XRD evidence and the Pd sintering observed by STEM. Based on the presence of the Pd–Pd shell, we can observe that 2Pd/YFO-A_T also exhibits a contribution from metallic Pd that is evident from the small peak at *ca.* 2.5 Å. The presence of an additional scattering feature at 2.1 Å in the FT-EXAFS data of 2Pd/YFO-A_S could be assigned to the formation of a Pd–Fe alloy.[48]

The dispersion of Pd particles was also qualitatively characterized by CO adsorption using infrared spectroscopy (Fig. 4). After reduction of the fresh catalysts at 300 °C, adsorbed CO on Pd exhibits three main signals at 2090 cm^{-1} (linearly bonded CO on Pd^0 corner atoms, CO_L), 2000–1950 cm^{-1} (μ_2-bridge bonded species on Pd(100) facets or edge sites) and 1950–1800 cm^{-1} (a broad band resulting from μ_3-hollow/multiple bonded CO on Pd(111) planes) which were assigned according to the available literature.[71,74,75] Pd/ACZ-A_S is the only sample displaying a signal at 2125 cm^{-1} that could be attributed either to the presence of ionic $Pd^{\delta+}$ (ref. 76) or to coordination of CO to Ce^{3+}.[77] The major difference between the spectra of fresh 2Pd/YFO, 0.5Pd/YFO and Pd/ACZ lies in the overall intensity of the signals (Fig. 4), which varies in the order Pd/ACZ > 2Pd/YFO > 0.5Pd/YFO. The higher intensity of Pd/ACZ-F signals is caused by its larger specific surface area (Table 1), since more Pd can be probed by CO and by the IR radiation, whereas the larger intensity of signals of 2Pd/YFO-F over those of 0.5Pd/YFO-F is attributed to the difference in Pd loading at identical surface area values. The intensity ratio between the signals of CO_L and that of bridge-bonded CO (A_{2090}/A_{1990}) can be taken as an indicator of the contribution of CO adsorbed on Pd particle edges and corners relative to terrace sites. A larger A_{2090}/A_{1990} ratio corresponds to a smaller average particle size, which correlates well with the particle size trends measured from STEM images (Table 1). 0.5Pd/YFO-F exhibits the largest A_{2090}/A_{1990} ratio among all samples, thus explaining the difficulty in estimating its Pd particle size from STEM (Fig. 2g).

Ageing causes a severe loss of IR signal intensity in Pd/ACZ (note the scale bar in Fig. 4) and of the A_{2090}/A_{1990} intensity ratio, reflecting the loss of Pd dispersion. The intensity changes associated with the YFO-based catalysts are

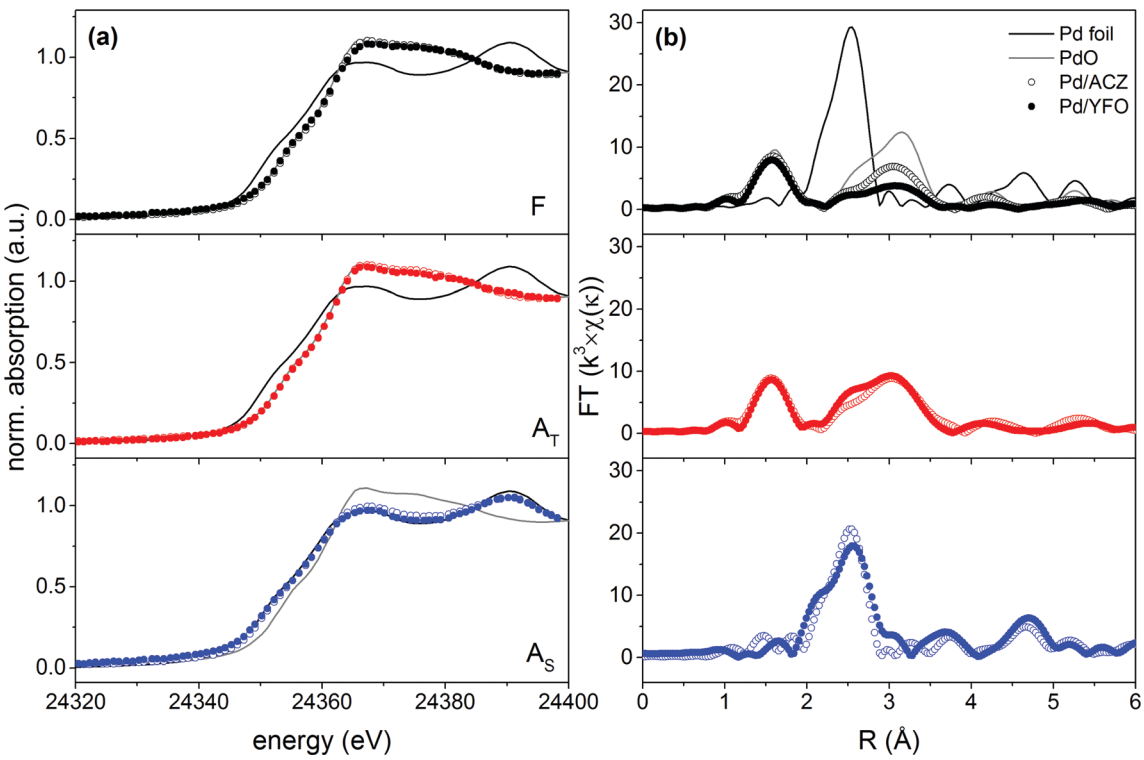

Fig. 3 (a) XANES and (b) non-phase shift corrected k^3-weighted FT-EXAFS spectra of fresh and aged 2Pd/YFO and Pd/ACZ. F, fresh; A_T, thermal ageing; A_S, stoichiometric ageing.

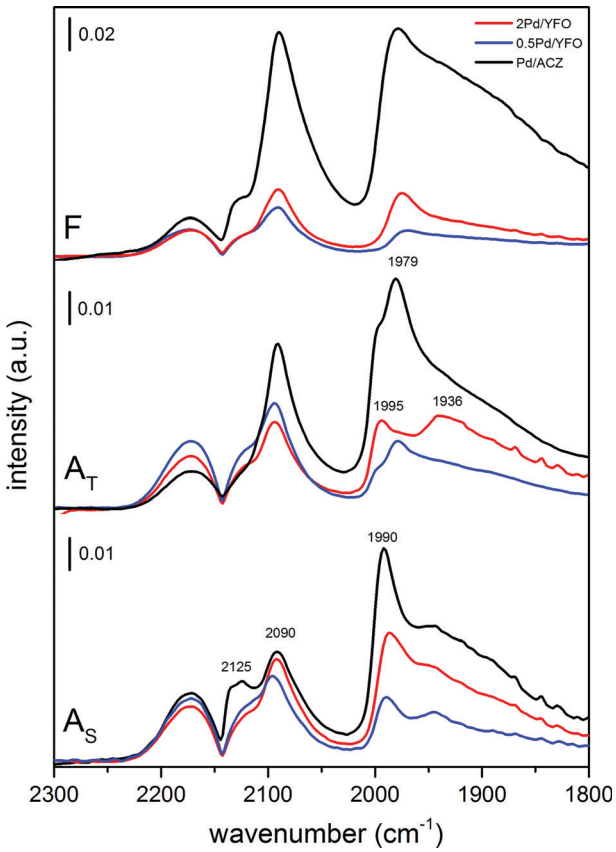

Fig. 4 DRIFTS spectra of adsorbed CO on fresh and aged 2Pd/YFO, 0.5Pd/YFO and Pd/ACZ. F, fresh; A_T, thermal ageing; A_S, stoichiometric ageing.

strikingly less evident. The position of the signals corresponding to CO_L (2090 cm^{-1}) and hollow bonded CO (1930–1800 cm^{-1}) in the aged samples is similar to those observed in fresh catalysts. The signals of the bridge-bonded CO species vary more significantly from stoichiometric ageing to thermal ageing. In the A_S catalysts, the signal is slightly shifted to 1990 cm^{-1} compared to fresh samples (1980 cm^{-1}), but spectra of 2Pd/YFO-A_S, 0.5Pd/YFO-A_S and Pd/ACZ-A_S are very similar, likely reflecting a comparable morphology but different sizes of the Pd particles. Two to three signals corresponding to μ_2-bridge-bonded CO species are visible below 2000 cm^{-1} in the spectra of A_T catalysts. 2Pd/YFO-A_T presents a pronounced signal at *ca.* 1936 cm^{-1} that could be assigned to isolated bridge species.[77,78] Comparison between STEM and DRIFTS data for these catalysts is also more difficult. STEM suggests the presence of large PdO particles (confirmed by EXAFS) that are challenging to clearly detect, whereas pre-reduction of the samples prior to CO adsorption may affect the aspect of the particles. Reduction of the large PdO particles of 2Pd/YFO-A_T may cause the formation of islands of metallic Pd that could account for the signal at 1936 cm^{-1}. Therefore, the difference between the spectra of A_T and A_S catalysts is attributed to the different morphologies obtained after reduction at 300 °C.

Time-resolved high energy XRD

The surface dynamics of the fresh and aged catalysts was addressed using high energy X-ray diffraction combined with the modulation excitation approach.[61,79] High energy XRD is a suitable method because it provides information on the whole material in a snapshot and in a time-resolved manner. It has been shown that subtle structural changes occurring during reaction that are not visible in XRD can be enhanced if the experimental data are collected under pulsed conditions.[61]

In this work, the modulation experiment consists of alternate and repeated CO *vs.* O_2 pulses that should simulate the protocol typically used to determine the dynamic OSC.[80] We restrict the discussion to fresh and aged 2Pd/YFO catalysts whose time-resolved XRD patterns recorded at 400 °C are dominated by the hexagonal and orthorhombic $YFeO_3$ structures, respectively (Fig. 5a). Similarly to the XRD of Fig. 1, and despite the exposure to high temperature during ageing and the resulting structural changes mentioned above, there remains still no clear indication about the Pd-containing phase because of the systematic overlap of Pd and PdO reflections with those of the support oxide. A completely different picture is obtained from the phase-resolved data of Fig. 5b, where reversible structural variations during the CO–O_2 pulses become clearly visible. By comparison with ICSD diffraction data (Fig. 5b, top), the reflections that became visible at 2.78 $Å^{-1}$ (corresponding to 2θ = 40° for CuKα radiation) and 3.22 $Å^{-1}$ (46.5°) are assigned to Pd metal, whereas the broader features at 2.36 $Å^{-1}$ (33.6°) and 3.74 $Å^{-1}$ (54.6°) are assigned to PdO reflections. The assignment is also corroborated by the opposite sign of the signals of Pd and PdO. The reflections of the Pd-containing phases experience only an amplitude change in response to the modulation. On the contrary, the weaker changes associated with the dominant reflections of $YFeO_3$ involve both amplitude and *d* spacing variations. The signals exhibit a complex differential profile that is given by the overlap of various close reflections. In agreement with similar experiments conducted on Pd/ACZ,[61] the *d* spacing variation during the modulation experiment is associated with the OSC characteristics of the material, therefore oxygen release in CO (decrease of ***Q***) and oxygen uptake in O_2 (increase of ***Q***).

The major difference between the catalysts is the amplitude of the changes emphasized by PSD. The overall intensity of the changes observed in 2Pd/YFO-F is small compared to that of the aged catalysts. Only the oscillations of hexagonal $YFeO_3$(111) at 2.32 $Å^{-1}$ (2θ = 33°) and Pd(111) at 2.78 $Å^{-1}$ are obvious. This is due to lack of long range crystal order in the fresh catalyst because of the nano-size of the support and Pd. The reflection of Pd(111) in the fresh catalyst appears very broad for the same reason. The difference in the $YFeO_3$ crystal structure (hexagonal and orthorhombic) may also influence the extent of the observed changes related to the support oxide, because the surface oxygen content of the material is structure dependent.[67] The changes around the Pd and PdO reflections are most pronounced in 2Pd/YFO-A_S, whereas those associated with orthorhombic $YFeO_3$ are evident only in 2Pd/YFO-A_T

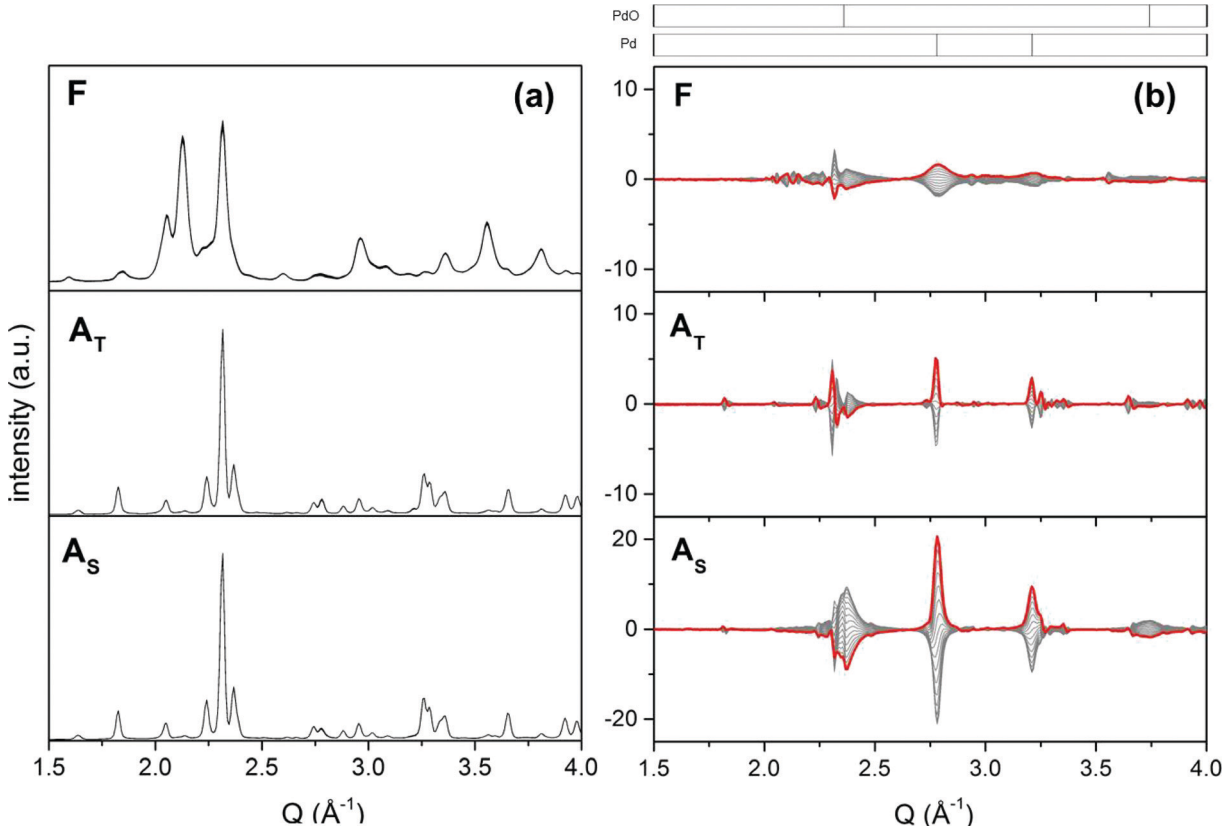

Fig. 5 (a) Time-resolved high energy XRD data of fresh and aged 2Pd/YFO obtained in a CO *vs.* O_2 modulation experiment at 400 °C. (b) Corresponding phase-resolved data. The red profile is the in-phase pattern. F, fresh; A_T, thermal ageing; A_S, stoichiometric ageing.

as a result of the lesser contribution from PdO. Thus, the oxygen exchange properties of the aged catalysts rely mainly on the oxidation and reduction of Pd particles in agreement with the above observations on the low OSCC values.[81] We cannot establish quantitatively how relevant is the structural variation observed for $YFeO_3$.

The temporal evolution of the Pd(200) reflection (3.22 $Å^{-1}$) for the three catalysts is reported in Fig. 6a. No kinetic data for the two $YFeO_3$ phases are shown because of the high level of noise and the very small changes induced by the modulation experiment that allow only for a qualitative evaluation of the data. Pd(200) is selected because the strongest Pd(111) reflection (2.78 $Å^{-1}$) interferes with those of the $YFeO_3$ phases, especially in 2Pd/YFO-A_T. The data also clearly evidence the difference in amplitude discussed above. It is clear from the kinetic data that the Pd and PdO reflections show opposite behavior in the phase-resolved data of Fig. 5b because Pd species reduce and re-oxidize in the CO–O_2 pulses. Besides the marked difference in amplitude of the changes, the delay at which changes occur in the CO pulse is also different. Whereas PdO of 2Pd/YFO-A_T reduces immediately in the presence of CO (Fig. 6a), the development of the Pd(200) reflection sets in only after *ca.* 10 s in 2Pd/YFO-F and 2Pd/YFO-A_S and is completed within a few seconds.

The structural changes are reversible and Pd re-oxidation occurs in all catalysts. However, it is a slower process than reduction and encompasses the whole O_2 pulse. The corresponding MS data (Fig. 6b) show that CO_2 evolution takes place over the whole CO pulse in the case of the fresh catalyst. In agreement with the temporal evolution of the Pd(200) reflection, the only little gas phase CO that is observed appears after *ca.* 10 s from admittance of CO and in correspondence of the decrease of CO_2 evolution. Therefore, 2Pd/YFO-F is the most active to oxidize CO, which is facilitated by the rather high SSA and high OSCC value compared to the aged catalysts (Table 1). Ageing causes an earlier CO breakthrough in the gas phase and a corresponding earlier breakthrough of gas phase O_2 in the oxidation pulse. However, 2Pd/YFO-A_S is able to consume CO up to about half the total duration of the CO pulse, a fact that is reflected in the broader CO_2 profile than that of 2Pd/YFO-A_T and which agrees well with the retarded Pd reduction observed in the high energy XRD data. Hence, in this type of experiment 2Pd/YFO-A_S demonstrates better oxygen storage capacity than 2Pd/YFO-A_T. The catalyst aged under stoichiometric conditions possesses highly reactive surface oxygen species giving high CO_2 evolution under oscillating conditions, whereas the thermally aged catalyst is characterized by poorer oxygen exchange properties. Given the similar structure of the support, this difference is associated with the redox properties of the metallic Pd particles of 2Pd/YFO-A_S. The discrepancy with the OSCC values is explained by the milder reduction conditions and the repeated redox pulses

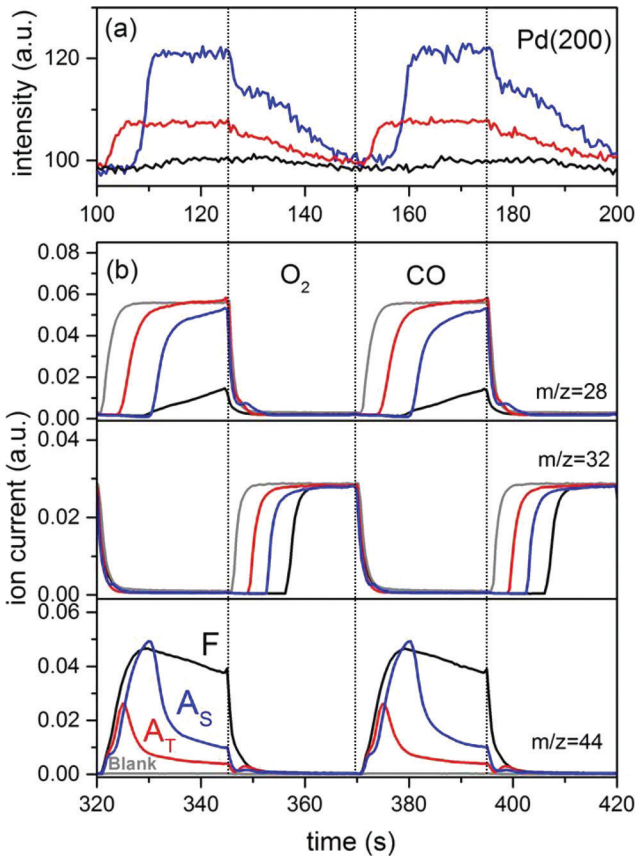

Fig. 6 (a) Temporal evolution of the Pd(200) reflection obtained from the time-resolved high energy XRD data of the CO *vs.* O_2 modulation experiment at 400 °C. (b) Corresponding online MS data. F, fresh; A_T, thermal ageing; A_S, stoichiometric ageing.

applied during the pulse experiment compared to the thermogravimetric experiment. Therefore, the metallic Pd particles observed on 2Pd/YFO-A_S appear crucial for maintaining the oxygen exchange properties of the catalyst.

Based on the Scherrer equation using the Pd(111) reflection of the in-phase XRD pattern of each catalyst (Fig. 5b, red), the estimation of the Pd crystallite size provides 2.6, 13.5 and 7.6 nm for 2Pd/YFO-F, 2Pd/YFO-A_T and 2Pd/YFO-A_S, respectively. The estimation is strongly affected by the assumption that all catalysts possess spherical (and unstrained) particles, which does not correspond to the STEM images especially in the case of 2Pd/YFO-A_T. Finally, the estimation is also affected by some overlap of the selected reflection with those of YFO_3. The values obtained considering these issues are lower than the particle size values determined by STEM (Table 1). The kinetic data of Fig. 6a indicate a slow re-oxidation that is possibly not able to involve the full particle volume. Hence, the estimation of the crystallite size based on the net variation of the Pd(200) reflection indicates that a large fraction of Pd but likely not all Pd responds to the CO–O_2 modulation, *i.e.* is repeatedly oxidized and reduced.

To conclude this section, high energy XRD data provide a qualitative measure of the facility of Pd to undergo a redox cycle. The large metallic Pd particles observed in 2Pd/YFO-A_S (*ca.* 20 nm) are subject to re-oxidation under periodic redox conditions at 400 °C suggesting that this could well be the situation also under stoichiometric reaction conditions.

Three-way catalytic activity

Fig. 7 shows the light-off curves of CH_4 obtained for fresh and aged catalysts under stoichiometric conditions. The T_{50} for CH_4 and T_{50} for CO ($T_{50}^{CH_4}$ and T_{50}^{CO}) are summarized in Table 2. A systematic improvement in $T_{50}^{CH_4}$ upon ageing is observed in the perovskite-type catalysts. Despite the structural changes observed after ageing involving both Pd and support particle growth, $T_{50}^{CH_4}$ of the 2Pd/YFO-A_S catalyst is shifted by more than 100 °C to lower temperature after stoichiometric ageing, attaining those of Pd/ACZ-F and Pd/ACZ-A_S. Similar activity improvement by nearly 80 °C is observed also for 0.5Pd/YFO-A_S. The effect of thermal ageing is less pronounced, but $T_{50}^{CH_4}$ is shifted by 50 °C to lower temperature in both YFO-based catalysts. For comparison, the activity of Pd/ACZ is stable upon ageing. Only thermal ageing increases $T_{50}^{CH_4}$ by 40 °C contrary to the behavior of Pd/YFO catalysts. This deactivation is attributed to the more significant sintering of PdO particles (Table 1). In contrast to Pd/ACZ, the aged YFO catalysts do not reach full CH_4 conversion at 800 °C, which is attributed to the low surface area of both the Pd and the $YFeO_3$ support and to the limited oxygen storage capacity of the aged catalysts.

Contrary to CH_4, CO oxidation activity of 2Pd/YFO, 0.5Pd/YFO and Pd/ACZ decreases upon ageing (Table 2) and the structural changes produced by thermal ageing appear more severe likely as a result of Pd particle growth.[82,83] This is in agreement with observations on Pd-based catalysts aged on a dynamometer.[84] Besides, the $YFeO_3$ support alone exhibited deactivation upon consecutive reaction runs.[53] Therefore, the activity enhancement is peculiar to CH_4 chemistry on Pd. The influence of water on the feedstock still remains to be assessed to ascertain whether a true activity enhancement would also be observed since water has been reported to decrease the catalytic activity of Pd.[85,86]

It is clear from the characterization and the activity data that activation is coincident with the formation of well-defined metallic Pd particles. Because of the similar structural changes, the activity improvement appears to be of the same nature as that observed for 2Pd/YFO-F during consecutive reaction cycles under stoichiometric conditions.[53] The formation of metallic Pd particles is accompanied by the loss of surface area of the catalyst and by the phase transition from hexagonal to orthorhombic $YFeO_3$. However, because the OSCC values after ageing seem to be associated with Pd rather than with the presence of $YFeO_3$, the support does not appear to be responsible for the improved catalytic activity after ageing. This indicates that the degree of coordination of Pd with $YFeO_3$ after prolonged exposure to 900 °C is low and likely not

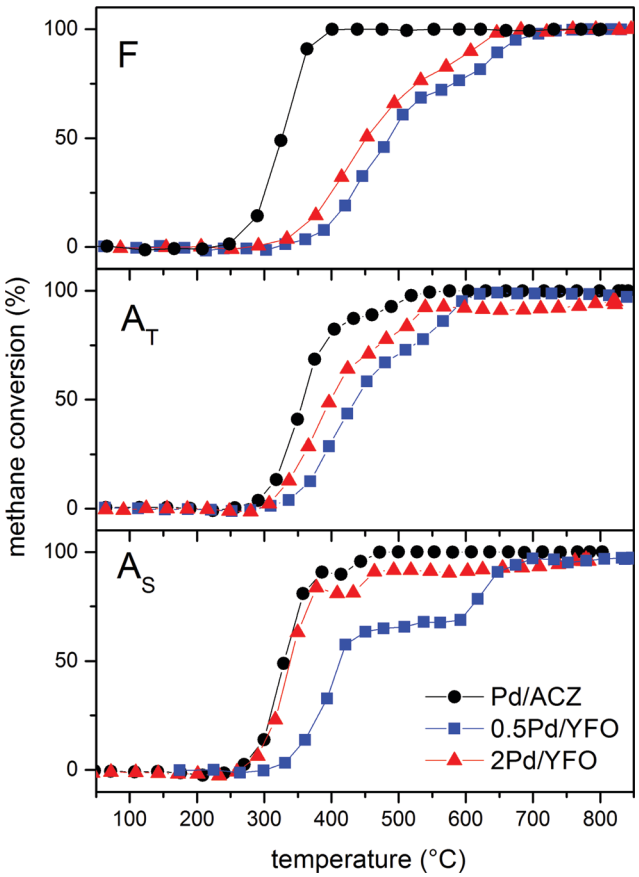

Fig. 7 CH_4 conversion curves of fresh and aged 2Pd/YFO, 0.5Pd/YFO and Pd/ACZ. F, fresh; A_T, thermal ageing; A_S, stoichiometric ageing.

Table 2 Catalytic activity of the fresh and aged catalysts

	$T_{50}^{CH_4}$ (°C)[a]			T_{50}^{CO} (°C)[b]		
Entry	F	A_T	A_S	F	A_T	A_S
Pd/ACZ	320	358	329	116	206	189
2Pd/YFO	452	399	338	164	228	204
0.5Pd/YFO	487	435	413	171	174	236

[a] Temperature of 50% CH_4 conversion. [b] Temperature of 50% CO conversion.

of the same 'self-regenerative' nature as $LaFeO_3$. The Pd–$YFeO_3$ interaction was shown to change already from a sample calcined at 700 °C to one calcined at 800 °C, the latter exposing PdO-like particles on hexagonal $YFeO_3$.[52] However, no phase transition was observed, indicating that the hexagonal structure may have been stabilized by the interaction with Pd. In contrast, $YFe_{1-x}Pd_xO_{3-\delta}$ (x = 0.1) was shown to be a self-regenerative catalyst for CO oxidation,[66] but no high temperature treatment was performed in previous studies. Our interpretation of the low temperature self-regeneration *versus* the high temperature segregation of Pd is in terms of geometric factors; however, this needs further confirmation. The periodic segregation–incorporation of Pd in $YFeO_3$ is favored at low temperature due to the fact that Pd can adopt a coordination similar to that of tetrahedral Fe ions of hexagonal $YFeO_3$.[51] In the flame-made catalyst, Pd is deposited on the $YFeO_3$ oxide already in the fresh state. Some extent of interaction is observed, but it is likely not sufficient to avoid the phase transition to orthorhombic $YFeO_3$.[53] In this phase, the segregation of Pd is favored because Y^{3+} (1.18 Å)[87] does not help in stabilizing a Pd^{3+}-like cation in the octahedral Fe sites, contrary to the larger La^{3+} (1.36 Å)[88] in $LaFeO_3$. The strong tendency of Pd^{3+} to disproportionate to Pd^{2+} and Pd^{4+}, when it is in an oxide lattice, can be overcome by the relatively small octahedral tilting due to the largest rare earth ion being in the A-site.[89]

It is tempting to associate the improved catalytic activity with metallic Pd based on the experimental observations. The particle size dependence (structure sensitivity) and the role of metallic Pd *vs.* PdO are still debated issues in methane oxidation.[4,19,90–95] This uncertainty is predominantly associated with the different experimental conditions used for the determination of catalytic activity and the difference in nature of the various catalysts. Moreover, the debate concerns primarily methane oxidation under lean conditions, where it is accepted that PdO is formed during reaction. Few studies have been reported for oxidation under low partial pressures of oxygen as it is the case for a TWC. The characterization data, together with the activity data of Fig. 7, demonstrate that discrete metal particles are favorable for methane oxidation, which is in agreement with various observations by others.[25,26,90] This is not only the case for 2Pd/YFO but also for the reference catalyst, a conventional TWC, where particle growth occurs despite the presence of ceria–zirconia, and the activity of Pd/ACZ-A_S is unchanged compared to that of Pd/ACZ-F. An important piece of information is derived from the observation that both the large Pd particles and the possibly large PdO particles undergo a reversible reduction–oxidation under redox conditions. Therefore, under the stoichiometric conditions used in this work, oxygen is activated on the large Pd particles of 2Pd/YFO-A_S. On the large PdO particles formed in the thermally aged Pd/YFO-A_T catalysts where an activity improvement is induced to a lesser extent, the activation phenomenon could be explained with the partial reduction of PdO during reaction, thus forming metallic Pd on the PdO surface.[30] EXAFS and DRIFTS data confirm this possibility. Therefore, a mixed PdO_x/Pd phase is present during reaction in both aged catalysts.

Finally, the light-off profiles of Pd/ACZ-A_S and 2Pd/YFO-A_S exhibit a clear loss of CH_4 conversion by 10–20% around 350–450 °C (Fig. 7). This is more pronounced in 0.5Pd/YFO-A_S (400–650 °C), likely as a consequence of the lower Pd content. This behaviour is characteristic of supported PdO catalysts under lean conditions and is due to spontaneous PdO reduction.[19,20,93] The activity loss is slightly more pronounced in the samples aged under stoichiometric conditions because of the presence of large metal particles, thus diminishing the amount of available Pd atoms. These particles can be partially oxidized as demonstrated above, but reduction during

reaction occurs at lower temperature because of the low oxygen content in the feed under $\lambda = 1$ conditions.[23] Further study under reaction conditions should be performed to confirm this behavior and the low temperature reduction of PdO.

Conclusions

The catalytic performance of Pd/YFO with 0.5 and 2 wt% Pd content was determined after high temperature treatment. Two ageing protocols were chosen, thermal ageing at 900 °C in air and stoichiometric ageing at 900 °C under reaction conditions comprising CH_4, CO, NO and oxygen. The reference TWC was aged under identical conditions for comparison. A gradual activity improvement was observed from the performance of the fresh Pd/YFO catalyst to the thermally aged one and to the sample aged under stoichiometric conditions. Pd loading affected only the extent of improvement, with the highest loading providing a better activity. After stoichiometric ageing, 2Pd/YFO was as active for methane oxidation as Pd/ACZ. In contrast to Pd/YFO catalysts, Pd/ACZ was less active after thermal ageing. For comparison, CO oxidation activity systematically decreased upon ageing indicating that the observed improved oxidation activity is peculiar to CH_4.

Structural characterization of the aged catalysts revealed that the activity improvement of Pd/YFO after stoichiometric ageing is accompanied by the formation of well-defined metallic Pd particles of *ca.* 20 nm. In the case of thermal ageing that produces less activity enhancement, Pd remains predominantly oxidized. The interaction of Pd with $YFeO_3$ is poorer after ageing probably as a result of the phase changes observed in the support that prevent coordination of Pd within the $YFeO_3$ lattice. Therefore, the observed activity improvement is mostly attributed to the changes related to the shape and oxidation state of Pd particles. However, it has been demonstrated that both Pd and $YFeO_3$ remain highly dynamic with respect to exposure to periodic redox conditions. Large metallic and oxidic Pd particles periodically reduce and oxidize. Therefore, this study provides evidence that a mixed PdO_x/Pd pair is at work during reaction and that large metal particles are not detrimental to methane oxidation under stoichiometric conditions.

Acknowledgements

Financial support from the Swiss National Science Foundation under project numbers 406240-1261274 (NRP62 'Smart materials') and 200021-138068 and the Centre for Materials Science and Technology (CCMX) is greatly appreciated. ESRF and SLS are acknowledged for beamtime allocation at beamlines ID15B and SuperXAS, respectively.

References

1 R. M. Heck, R. J. Farrauto and S. T. Gulati, *Catalytic air pollution control: Commercial technology*, Wiley, 3rd edn, 2009.
2 D. Ciuparu, M. R. Lyubovsky, E. Altman, L. D. Pfefferle and A. Datye, *Catal. Rev.: Sci. Eng.*, 2002, **44**, 593.
3 P. Gelin and M. Primet, *Appl. Catal., B*, 2002, **39**, 1.
4 D. Bounechada, G. Groppi, P. Forzatti, K. Kallinen and T. Kinnunen, *Top. Catal.*, 2013, **56**, 372.
5 Y. Lu, S. K. Matam, G. L. Chiarello, P. Dimopoulos Eggenschwiler, C. Bach, M. Weilenmann, A. Spiteri, A. Weidenkaff and D. Ferri, *Catal. Commun.*, 2013, **39**, 55.
6 M. Salaün, A. Kouakou, S. Da Costa and P. Da Costa, *Appl. Catal., B*, 2009, **88**, 386.
7 A. Winkler, A. Eyssler, A. Maegli, A. Liati, P. Dimopoulos Eggenschwiler and C. Bach, *Fuel*, 2013, **111**, 855.
8 S. K. Matam, E. H. Otal, M. H. Aguirre, A. Winkler, A. Ulrich, D. Rentsch, A. Weidenkaff and D. Ferri, *Catal. Today*, 2012, **184**, 237.
9 A. Winkler, D. Ferri and R. Hauert, *Catal. Today*, 2010, **155**, 140.
10 M. Honkanen, M. Kärkkäinen, V. Viitanen, H. Jiang, K. Kallinen, M. Huuhtanen, M. Vippola, J. Lahtinen, R. Keiski and T. Lepistö, *Top. Catal.*, 2013, **56**, 576.
11 J. Chen, R. M. Heck and R. J. Farrauto, *Catal. Today*, 1992, **11**, 517.
12 J. Andersson, M. Antonsson, L. Eurenius, E. Olsson and M. Skoglundh, *Appl. Catal., B*, 2007, **72**, 71.
13 D. L. Mowery, M. S. Graboski, T. R. Ohno and R. L. McCormick, *Appl. Catal., B*, 1999, **21**, 157.
14 M. J. Rokosz, A. E. Chen, C. K. Lowe-Ma, A. V. Kucherov, D. Benson, M. C. P. Peck and R. W. McCabe, *Appl. Catal., B*, 2001, **33**, 205.
15 R. Burch and F. J. Urbano, *Appl. Catal., A*, 1995, **124**, 121.
16 N. van Vegten, M. Maciejewski, F. Krumeich and A. Baiker, *Appl. Catal., B*, 2009, **93**, 38.
17 S. Colussi, A. Trovarelli, G. Groppi and J. Llorca, *Catal. Commun.*, 2007, **8**, 1263.
18 M. Cargnello, J. J. Delgado Jaen, J. C. Hernandez Garrido, K. Bakhmutsky, T. Montini, J. J. Calvino Gamez, R. J. Gorte and P. Fornasiero, *Science*, 2012, **337**, 713.
19 R. J. Farrauto, J. K. Lampert, M. C. Hobson and E. M. Waterman, *Appl. Catal., B*, 1995, **6**, 263.
20 J. G. McCarty, *Catal. Today*, 1995, **26**, 283.
21 R. J. Farrauto, M. C. Hobson, T. Kennelly and E. M. Waterman, *Appl. Catal., A*, 1992, **81**, 227.
22 R. J. Farrauto, M. C. Hobson, T. Kennelly and E. M. Waterman, *Appl. Catal., A*, 1992, **81**, 227.
23 S. K. Matam, G. L. Chiarello, Y. Lu, A. Weidenkaff and D. Ferri, *Top. Catal.*, 2013, **56**, 239.
24 S. B. Kang, S. J. Han, S. B. Nam, I. S. Nam, B. K. Cho, C. H. Kim and S. H. Oh, *Top. Catal.*, 2013, **56**, 298.
25 A. Y. Stakheev, A. M. Batkin, N. S. Teleguina, G. O. Bragina, V. I. Zaikovsky, I. P. Prosvirin, A. K. Khudorozhkov and V. I. Bukhtiyarov, *Top. Catal.*, 2013, **56**, 306.
26 A. Baylet, P. Marecot, D. Duprez, P. Castellazzi, G. Groppi and P. Forzatti, *Phys. Chem. Chem. Phys.*, 2011, **13**, 4607.
27 S. K. Matam, M. H. Aguirre, A. Weidenkaff and D. Ferri, *J. Phys. Chem. C*, 2010, **114**, 9439.
28 P. Briot and M. Primet, *Appl. Catal.*, 1991, **68**, 301.

29 D. Ciuparu and L. Pfefferle, *Appl. Catal., A*, 2001, **218**, 197.
30 S. C. Su, J. N. Carstens and A. T. Bell, *J. Catal.*, 1998, **176**, 125.
31 S. Royer and D. Duprez, *ChemCatChem*, 2011, **3**, 24.
32 M. A. Pena and J. L. G. Fierro, *Chem. Rev.*, 2001, **101**, 1981.
33 W. F. Libby, *Science*, 1971, **171**, 499.
34 R. J. H. Voorhoeve, J. P. Remeika and D. W. J. Johnson, *Science*, 1973, **180**, 62.
35 C. H. Kim, G. Qi, K. Dahlberg and W. Li, *Science*, 2010, **327**, 1624.
36 Y. Nishihata, J. Mizuki, T. Akao, H. Tanaka, M. Uenishi, M. Kimura, T. Okamoto and N. Hamada, *Nature*, 2002, **418**, 164.
37 N. Guilhaume and M. Primet, *J. Catal.*, 1997, **165**, 197.
38 K. Zhou, H. Chen, Q. Tian, Z. Hao, D. Shen and X. Xu, *J. Mol. Catal. A: Chem.*, 2002, **189**, 225.
39 D. Fino, *Sci. Technol. Adv. Mater.*, 2007, **8**, 93.
40 D. Fino, N. Russo, G. Saracco and V. Specchia, *Prog. Solid State Chem.*, 2007, **35**, 501.
41 Y. Chang and J. G. McCarty, *Catal. Today*, 1996, **30**, 163.
42 S. Royer, H. Alamdari, D. Duprez and S. Kaliaguine, *Appl. Catal., B*, 2005, **58**, 273.
43 M. Uenishi, M. Taniguchi, H. Tanaka, M. Kimura, Y. Nishihata, J. Mizuki and T. Kobayashi, *Appl. Catal., B*, 2005, **57**, 267.
44 M. Casapu, J. D. Grunwaldt, M. Maciejewski, A. Baiker, S. Eckhoff, U. Göbel and M. Wittrock, *J. Catal.*, 2007, **251**, 28.
45 M. B. Katz, G. W. Graham, Y. Duan, H. Liu, C. Adamo, D. G. Schlom and X. Pan, *J. Am. Chem. Soc.*, 2011, **133**, 18090.
46 H. Tanaka, M. Taniguchi, M. Uenishi, N. Kajita, I. Tan, Y. Nishihata, J. Mizuki, K. Narita, M. Kimura and K. Kaneko, *Angew. Chem., Int. Ed.*, 2006, **45**, 5998.
47 Y. Lu, A. Eyssler, E. H. Otal, S. K. Matam, O. Brunko, A. Weidenkaff and D. Ferri, *Catal. Today*, 2013, **208**, 42.
48 J. A. Kurzman, J. Li, T. D. Schladt, C. R. Parra, X. Ouyang, R. Davis, J. T. Miller, S. L. Scott and R. Seshadri, *Chem. Mater.*, 2011, **50**, 8073.
49 I. Tan, H. Tanaka, M. Uenishi, K. Kaneko and S. Mitachi, *J. Ceram. Soc. Jpn.*, 2005, **113**, 71.
50 J. P. Dacquin, M. Cabie, C. R. Henry, C. Lancelot, C. Dujardin, S. R. Raouf and P. Granger, *J. Catal.*, 2010, **270**, 299.
51 J. Li, U. G. Singh, T. D. Schladt, J. K. Stalick, S. L. Scott and R. Seshadri, *Chem. Mater.*, 2008, **20**, 6567.
52 A. Eyssler, A. Winkler, O. Safonova, M. Nachtegaal, S. K. Matam, P. Hug, A. Weidenkaff and D. Ferri, *Chem. Mater.*, 2012, **24**, 1864.
53 Y. Lu, K. A. Michalow, S. K. Matam, A. Winkler, A. E. Maegli, S. Yoon, A. Heel, A. Weidenkaff and D. Ferri, *Appl. Catal., B*, 2014, **144**, 631.
54 S. Yoon, S. Hua, N. Y. Kado, A. Thiruvengadam, J. F. Collins, M. Gautam, J. D. Herner and A. Ayala, *Atmos. Environ.*, 2014, **83**, 220.
55 E. Tzimpilis, N. Moschoudis, M. Stoukides and P. Bekiaroglou, *Appl. Catal., B*, 2009, **87**, 9.
56 S. J. Pennycook, *Ultramicroscopy*, 1989, **30**, 58.
57 W. S. Rasband, U.S. National Institutes of Health, Bethesda, Maryland, USA, 1997–2012, imagej.nih.gov/ij/.
58 E. Mamontov, R. Brezny, M. Koranne and T. Egami, *J. Phys. Chem. B*, 2003, **107**, 13007.
59 A. Pappacena, K. Schermanz, A. Sagar, E. Aneggi and A. Trovarelli, *Stud. Surf. Sci. Catal.*, 2010, **175**, 835.
60 B. Ravel and M. Newville, *J. Synchrotron Radiat.*, 2005, **12**, 537.
61 D. Ferri, M. A. Newton, M. Di Michiel, S. Yoon, G. L. Chiarello, V. Marchionni, S. K. Matam, M. H. Aguirre, A. Weidenkaff, F. Wen and J. Gieshoff, *Phys. Chem. Chem. Phys.*, 2013, **15**, 8629.
62 D. Baurecht and U. P. Fringeli, *Rev. Sci. Instrum.*, 2001, **72**, 3782.
63 A. Urakawa, T. Bürgi and A. Baiker, *Chem. Eng. Sci.*, 2008, **63**, 4902.
64 D. Ferri, S. K. Matam, R. Wirz, A. Eyssler, O. Korsak, P. Hug, A. Weidenkaff and M. A. Newton, *Phys. Chem. Chem. Phys.*, 2010, **12**, 5634.
65 D. Chernyshov, W. van Beek, H. Emerich, M. Milanesio, A. Urakawa, D. Viterbo, L. Palin and R. Caliandro, *Acta Crystallogr., Sect. A: Found. Crystallogr.*, 2011, **67**, 327.
66 J. Li, U. G. Singh, T. D. Schladt, J. K. Judith, S. L. Scott and R. Seshadri, *Chem. Mater.*, 2008, **20**, 6567.
67 L. Wu, J. C. Yu, L. Zhang, X. Wang and S. Li, *J. Solid State Chem.*, 2004, **177**, 3666.
68 Y. Zhang, J. Yang, J. Xu, Q. Gao and Z. Hong, *Mater. Lett.*, 2012, **81**, 1.
69 T. Suzuki, A. Morikawa, A. Suda, H. Sobukawa, M. Sugiura, T. Kanazawa, J. Suzuki and T. Takada, *Toyota Chuo Kenkyusho R&D Rebyu*, 2002, **37**, 28.
70 N. M. Rodriquez, S. G. Oh, R. A. Dalla-Betta and R. T. K. Baker, *J. Catal.*, 1995, **157**, 676.
71 T. Lear, R. Marshall, J. A. Lopez-Sanchez, S. D. Jackson, T. M. Klapötke, M. Bäumer, G. Rupprechter, H. J. Freund and D. Lennon, *J. Chem. Phys.*, 2005, **123**, 1.
72 S. K. Matam, E. V. Kondratenko, M. H. Aguirre, P. Hug, D. Rentsch, A. Winkler, A. Weidenkaff and D. Ferri, *Appl. Catal., B*, 2013, **129**, 214.
73 R. Rohé and V. Pitchon, *Top. Catal.*, 2001, **16/17**, 311.
74 P. Gelin, A. R. Siedle and J. T. Yates, *J. Phys. Chem.*, 1984, **88**, 2978.
75 D. Tessier, A. Rakai and F. Bozon-Verduraz, *J. Chem. Soc., Faraday Trans.*, 1992, **88**, 741.
76 A. Palazov, C. C. Chang and R. J. Kokes, *J. Catal.*, 1975, **36**, 338.
77 C. Binet, A. Badri and J. C. Lavalley, *J. Phys. Chem.*, 1994, **98**, 6392.
78 W. Daniell, H. Landes, N. E. Fouad and H. Knözinger, *J. Mol. Catal. A: Chem.*, 2002, **178**, 211.
79 R. Caliandro, D. Chernyshov, H. Emerich, M. Milanesio, L. Palin, A. Urakawa, W. van Beek and D. Viterbo, *J. Appl. Crystallogr.*, 2012, **45**, 458.
80 M. Boaro, F. Giordano, S. Recchia, V. DalSanto, M. Giona and A. Trovarelli, *Appl. Catal., B*, 2004, **52**, 225.
81 R. W. McCabe and R. K. Usmen, *Stud. Surf. Sci. Catal.*, 1996, **101**, 355.
82 R. Meyer, S. K. Shaikhutdinov and H. J. Freund, *Z. Phys. Chem.*, 2004, **218**, 905.
83 Z. W. Wang, B. Li, M. S. Chen, W. Z. Weng and H. L. Wan, *Sci. China: Chem.*, 2010, **53**, 2047.

84 J. H. Baik, H. J. Kwon, Y. T. Kwon, I. S. Nam and S. H. Oh, *Top. Catal.*, 2007, **42–43**, 337.
85 D. Ciuparu and L. Pfefferle, *Appl. Catal., A*, 2001, **209**, 415.
86 C. F. Cullis, T. G. Nevell and D. L. Trimm, *J. Chem. Soc., Faraday Trans.*, 1972, **68**, 1406.
87 X. Cao, C.-S. Kim and H.-I. Yoo, *J. Am. Ceram. Soc.*, 2001, **84**, 1265.
88 R. D. Shannon, *Acta Crystallogr., Sect. A: Cryst. Phys., Diffr., Theor. Gen. Crystallogr.*, 1976, **32**, 751.
89 S. J. Kim, S. Lemaux, G. Demazeau, J. Y. Kim and J. H. Choy, *J. Mater. Chem.*, 2002, **12**, 995.
90 R. F. Hicks, H. Qi, M. L. Young and R. G. Lee, *J. Catal.*, 1990, **122**, 280.
91 R. F. Hicks, H. Qi, M. L. Young and R. G. Lee, *J. Catal.*, 1990, **122**, 295.
92 T. R. Baldwin and R. Burch, *Appl. Catal.*, 1990, **66**, 359.
93 K. Persson, A. Ersson, S. Colussi, A. Trovarelli and S. G. Järas, *Appl. Catal., B*, 2006, **66**, 175.
94 H. Arai, T. Yamada, K. Eguchi and T. Seiyama, *Appl. Catal.*, 1986, **26**, 265.
95 J. R. Theis and R. W. McCabe, *Catal. Today*, 2012, **184**, 262.